Melilite LaSrGa3−xAlxO7 series: A combined solid-state NMR and neutron diffraction study

ARTICLE *in* THE JOURNAL OF PHYSICAL CHEMISTRY C · JUNE 2014

Impact Factor: 4.77 · DOI: 10.1021/jp504829x

6 AUTHORS, INCLUDING:

Andrew Pell
University of Cambridge
21 PUBLICATIONS **446** CITATIONS

THE JOURNAL OF PHYSICAL CHEMISTRY C

Article

pubs.acs.org/JPCC

Melilite $LaSrGa_{3-x}Al_xO_7$ Series: A Combined Solid-State NMR and Neutron Diffraction Study

Chiara Ferrara,[†] Cristina Tealdi,[†] Piercarlo Mustarelli,*[,†] Markus Hoelzel,[‡] Andrew J. Pell,[§,∥] and Guido Pintacuda[§]

[†]Department of Chemistry, University of Pavia, and INSTM, Via Taramelli 12, I-27100 Pavia, Italy

[‡]Forschungsneutronenquelle Heinz Maier-Leibnitz (FRM II), Technische Universität München, Lichtenbergstrasse 1, D-85747 Garching, Germany

[§]Centre de RMN à Très Hauts Champs, Institut des Sciences Analytiques, Université de Lyon (ENS-Lyon, UCB Lyon 1, CNRS UMR 5280), 5 rue de la Doua, 69100 Villeurbanne, France

Supporting Information

ABSTRACT: Oxides characterized by a layered melilite structure, with general formula $ABT^1_{(1)}T^2_{(2)}O_7$, find applications in many different technological fields due to their relevant magnetic, optical, and electrical properties. These functional properties are, in turn, related to local features such as structural defects and cation substitutions. Therefore, a complete structural characterization of these complex anisotropic compounds is mandatory, and the combined use of long-range (X-ray and neutron diffraction) and short-range (solid state NMR) techniques is a key approach to this aim. In this work, we present the full structural characterization of the series $LaSrGa_{3-x}Al_xO_7$ (x = 0, 1, 1.5, 2, and 3), which was obtained for the first time by means of a new sol−gel approach. Analysis of neutron diffraction data revealed that the distribution of La/Sr and Ga/Al on the respective sites is random. ^{27}Al and ^{71}Ga solid state NMR enabled us to rationalize the local structure of the T sites in terms of nearest and next-nearest neighbors. This study provides a deep structural insight that can be helpful for the understanding of the functional properties and is a powerful strategy for the analysis of complex oxide systems.

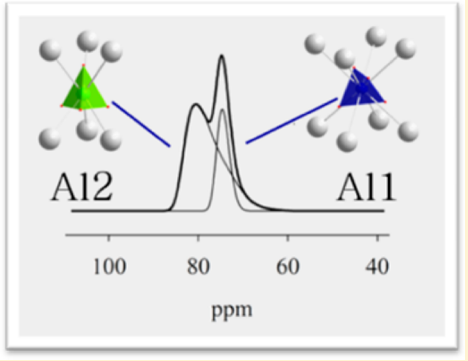

INTRODUCTION

Oxides with a layered melilite structure find applications in many different technological fields due to their varied optical and electrical properties. The melilite structure has the general formula $ABT^1_{(1)}T^2_{(2)}O_7$ where A is a large divalent alkaline earth cation, B a trivalent lanthanide on the same crystallographic site, M, and T^1 and T^2 are two distinct crystallographic sites that can be occupied by one or two different cations such as Si^{4+}, Ga^{3+}, Al^{3+}, Zn^{2+}, and Co^{2+}. The structure crystallizes in the tetragonal $P\bar{4}2_1m$ space group. The two-dimensional layers are composed of corner-sharing T^1O_4 and T^2O_4 tetrahedra which form tunnels thanks to their particular 5-fold connection; these layers are spaced by slabs of $(A/B)_2$ cations accommodated at the top and bottom of the tunnels. This layered structure allows a high degree of substitution, doping, and cation exchange on all the cationic sites A/B, T^1, and T^2. The properties of these systems are thus highly tunable, leading to a large variety of compounds with relevant properties for applications in many different fields.

$LaSrGa_3O_7$ has been used as a substrate for epitaxial growth of films of HT superconductors and laser materials.[1,2] At present, it is also under study as a possible electrolyte for solid-oxide fuel cells (SOFCs).[1,3] As a matter of fact, it becomes an interstitial oxide ion conductor when excess oxygen is introduced within the structure by modifying the cation stoichiometry to $La_{1+x}Sr_{1-x}Ga_3O_{7+\delta}$, ($\delta = x/2$), where $x \leq 0.5$.[3,4] The interstitial oxygen ions are accommodated between the layers within the 5-fold channels. Whereas the average structure has been completely solved,[3,4] the local structure and the distortions introduced by the presence of defects still need to be explained. Both theoretical and experimental approaches have been tried, leading to different models.[4−6]

Al-based melilites find applications in the field of optics.[7,8] In particular, adjustable optical properties can be obtained by proper doping with rare-earth[8,9] and substitutions on the A/B site. Also substitutions on the T^1 and T^2 sites are possible, which lead to the huge family of the Al−Si melilites. This family of compounds also finds application in the field of solid-state lasers,[8,10,15] phosphors, and photo luminescence[7] and LED technology.[11] The Al−Si system is relevant also in geophysics.[12] As a matter of fact, Al−Si-based compounds received great attention in the past since aluminosilicates are the constituents

Received: May 16, 2014
Revised: June 11, 2014
Published: June 12, 2014

   dx.doi.org/10.1021/jp504829x | J. Phys. Chem. C 2014, 118, 15036−15043

of many relevant structural materials (clay minerals, zeolites, and concrete),[13,14] and their study is fundamental for technological applications.[15,16] The gehlenite $Ca_2Al_2SiO_7$ compound has received great attention over the past few decades and recently has been reanalyzed to understand the particular ordered $Ca_2Al(AlSi)_2O_7$ structure characterized by specific constraints for the linkage between Al and Si tetrahedra.[17]

In consideration of these examples, it is clear that structure and the chemical and physical properties of melilite-type compounds are dominated by the peculiar anisotropy of the structure and by the presence of defects, such as substitutions, which influence the local order. Therefore, for a better understanding of the melilite properties, it is mandatory to address the differences between local and average structure. In this work, a combined diffractometric (neutron diffraction) and spectroscopic [solid-state nuclear magnetic resonance (NMR)] study of the series $LaSrGa_{3-x}Al_xO_7$ with $x = 0$, 1, 1.5, 2, and 3 is reported for the first time. The two end members of the series have already been investigated for their relevant properties, but a complete structural determination is still lacking. In particular, the complete solid solution had hitherto never been prepared. The aim of this study is to investigate the differences between the average and the local structure of this series of melilite compounds where two sources of disorder are present: the distribution of La and Sr on a single crystallographic site and the distribution of Ga and Al over two distinct sites. Different structural models are considered, and our previous study on the $LaSrAl_3O_7$ system[18] is used to address the problem of the La/Sr distribution. The use of neutron diffraction allows us to better determine the position of Ga/Al within the system thanks to their different neutron cross sections. Solid-state NMR is used to shed light on the differences between local and average structure.

EXPERIMENTAL SECTION

Syntheses were performed according to a sol−gel procedure. Polycrystalline samples of the series $LaSrGa_{3-x}Al_xO_7$ with $x = 0$, 1, 1.5, 2, and 3 were prepared starting from stoichiometric amounts of La_2O_3 (Sigma, 99.9% previously heated overnight at 1000 °C in order to eliminate absorbed water and carbon dioxide), Ga_2O_3 (Sigma, >99.0%), $Sr(NO_3)_2$ (Sigma, >99.0%), and $Al(NO_3)_2{\cdot}9H_2O$ (Sigma, 98.0%). La_2O_3 and Ga_2O_3 were dissolved in a solution of concentrated nitric acid at ∼100 °C and vigorously stirred. Stoichiometric amounts of $Sr(NO_3)_2$ and $Al(NO_3)_2{\cdot}9H_2O$ were then added together with an excess of citric acid as the chelating agent and ethylene glycol as the gelation agent. Mixing at 100 °C was carried out until a stable gel was obtained under continuous stirring. After complete evaporation of the water, the gel was heated to 1000 °C overnight to eliminate the organic components and the nitrogen residue. The resulting powder was pressed and heated at 1200 °C for 20 h and 1400 °C for 6 h with intermediate grinding.

Preliminary X-ray Diffraction (XRD) patterns of the samples were collected at ambient temperature using a Bruker D8 powder diffractometer (Cu Kα radiation) operating in Bragg−Brentano θ−θ geometry. The data were recorded in the 2θ range of 10−100° with a step size of 0.02 (2θ) and a constant counting time of 10 s per step.

Room temperature neutron diffraction data were acquired on the high-resolution powder diffractometer SPODI at Forschungs−Neutronenquelle Heinz Maier-Leibnitz (FRM II) in Garching (Germany).[19] The samples were investigated at room temperature using an automatic sample changer, which is a carousel hosting up to six vanadium sample cans. As the coherent scattering cross section of vanadium is close to zero, the scattering power of vanadium is practically negligible compared to the samples. The data were collected in the angular range of 0−160° with 0.05° stepwidth and a wavelength of 1.5483 Å using a Germanium(551) monochromator. The patterns were analyzed according to the Rietveld refinement method[20,21] with the use of the FullProf software package.[22] The refined parameters were the zero shift, scale factor, background, lattice parameters, atomic positions, isotropic, and where appropriate, anisotropic thermal factors.

Solid-state ^{27}Al Magic Angle Spinning (MAS) NMR spectra were collected on a Bruker Avance III 1000 spectrometer operating at a magnetic field of 23.5 T, and ^{27}Al Larmor frequency of 260.602 MHz on a 2.5 mm HX probe. All the spectra were collected at room temperature and referenced to a standard aqueous solution of 0.1 M $Al(NO_3)_3$ (0 ppm). Magic-angle spinning (MAS) spectra at 30 kHz were recorded using a one-pulse sequence with a central-transition-selective pulse of 1.67 μs (with a nominal RF field amplitude of 50 kHz, corresponding to a nominal flip angle of 30°) and 64 scans. Two-dimensional (2D) rotor-synchronized z-filtered triple-quantum MQMAS spectra were also acquired. High-power pulses of lengths 6.0 and 4.0 μs were used for the generation of triple quantum coherences and their conversion to z-magnetization, respectively, while a selective pulse of length 3.33 μs (with a nominal RF field amplitude of 25 kHz, corresponding to a nominal flip angle of 30°) was employed for the excitation of the central transition. The z-filter delay was 200 μs. The 2D spectra were acquired with 256 increments in the indirect dimension and between 24 and 216 scans per increment.

^{71}Ga MAS NMR spectra were collected on a Bruker Avance III 1000 spectrometer operating at a magnetic field of 23.5 T and a ^{71}Ga Larmor frequency of 305.007 MHz, equipped with a 2.5 mm probe. All the spectra were collected at room temperature, and the chemical shifts were referenced to a standard aqueous solution of 1.0 M $Ga(NO_3)_3$ (0 ppm). Spectra at 30 kHz MAS were recorded using a one-pulse sequence with a 2.5 μs (with a nominal RF field amplitude of 50 kHz, corresponding to a nominal flip angle of 45°); 1024−2048 scans were acquired. All the spectra were processed using TopSpin 3.0 (Bruker). The spectra were fitted with both TopSpin 3.0 SOLA (Bruker) and QuadFit packages.[23]

The components of the series $LaSrGa_{3-x}Al_xO_7$ will be named Ga3 ($x = 0$), Ga2Al1 ($x = 1$), Ga15Al15 ($x = 1.5$), Ga1Al2 ($x = 2$), and Al3 ($x = 3$) in the following.

RESULTS AND DISCUSSION

Figure 1 presents the neutron diffraction patterns for all the samples of the series $LaSrGa_{3-x}Al_xO_7$ with $x = 0$, 1, 1.5, 2, 3. All the patterns can be indexed in terms of the space group ($n113$) $P\text{-}42_1m$ already proposed in literature[3,4,18] and no evident distortions or deviations from the tetragonal symmetry are present; structural parameters are presented in Table S1 of the Supporting Information. The samples are generally characterized by a single phase; only for compositions Ga1Al2 and Al3 are any impurities noticeable (see below). From a first inspection of the patterns, it is possible to observe a clear trend of both peaks positions and intensities of selected peaks with composition (Figure 1, part b). In particular, substitution of Ga for Al leads to a peaks shift to lower angles, which corresponds

dx.doi.org/10.1021/jp504829x | J. Phys. Chem. C 2014, 118, 15036−15043

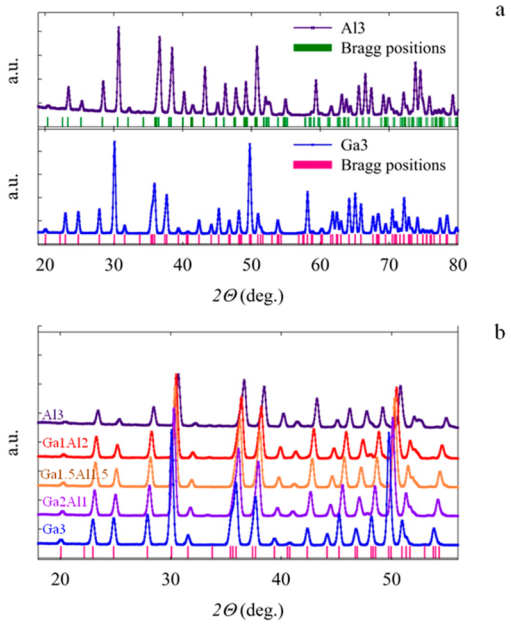

Figure 1. (a) Room temperature powder diffraction pattern for the two end members Ga3 and Al3 with corresponding Bragg positions; (b) zoom in the range of 18°−60° of the experimental neutron diffraction patterns for all the samples of the series $LaSrGa_{3-x}Al_xO_7$, where x = 0, 1, 1.5, 2, and 3; the trend in peaks positions and intensities with composition is highlighted. Bragg positions scheme refers to the x = 0 composition.

to the increase of the cell volume (see next Figure 5). Also the peaks intensities are affected by the composition: the peak intensity at ∼25° (reflection 201) increases with the Ga content while the intensity of the reflection at ∼43° (212 index) decreases with the raise of the Ga composition.

The sol−gel procedure allowed us to obtain the formation of the complete solid solution between the two end members Ga3 (pure Ga) and Al3 (pure Al). We stress that the syntheses of all the compounds were carried out without the necessity of empirical extra amounts of Ga, as reported in the literature to compensate for gallium volatilization during the prolonged high-temperature treatments when solid-state reactions were employed.[4,24] There, the optimal amounts of gallium extra quantities were determined empirically, and they were found to depend on the overall composition of the samples and on the duration of the treatment above 1400 °C (between 7 and 10 h for less than 1 g of product). Our sol−gel approach allowed us to reduce the length of the final step at high temperature and, at the same time, to prepare up to 4 g of sample in a single synthesis batch.

In order to obtain more detailed structural information, Rietveld refinements were performed. For the sample Ga1Al2 and Al3 additional low-intensity peaks at 2Θ values of ∼33°, 41°, 71°, and 85° were found. We identified the second phase as the perovskite $(La,Sr)AlO_3$. This perovskite structure has already been identified as a secondary phase in the synthesis of $LaSrGa_3O_7$ and $LaSrAl_3O_7$.[18,24] Two-phase refinements were then performed for these compositions from which we estimate the amount of the second phase to be approximately 2%. The presence of this minority phase will be neglected in the following.

The structural analysis for sample Ga3 and Al3 led to the average structure (tetragonal symmetry) reported in Figure 2,

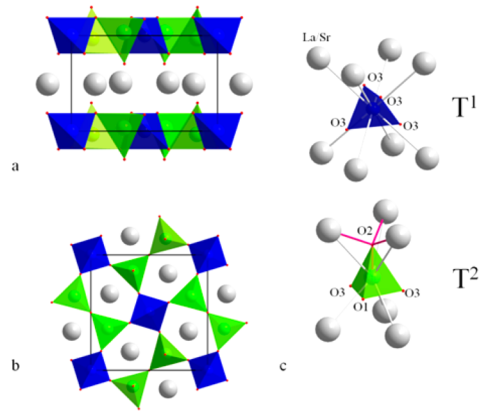

Figure 2. Melilite structure unit cell view along the (a) *b* axis and (b) *c* axis. T^1 (blue) and T^2 tetrahedra (green) are linked together in the *ab* plane. The planes are spaced by slabs of M cations (gray). (c) T^1 and T^2 sites (blue and green polyhedra) and cationic coordinations (white bonds). Pink bonds highlight the O^2 coordination with one T^2 site and three La/Sr sites.

which is in agreement with the literature.[1,18,25] In this structure, two distinct sites, namely T^1 and T^2, can be occupied by Ga and Al, so giving origin to a 2D tetrahedral network, and three different O positions are present, which will be named O^1, O^2, and O^3 in the following. La and Sr are distributed randomly over the same crystallographic site, M. The system is strongly anisotropic: the crystal structure consists of an alternate stack of the two-dimensional T_3O_7 layers and M planes along the *c* direction. The M ions are positioned at the centers of channels made of five tetrahedra, with the Ga and Al tetrahedra being connected to each other. The T^1 tetrahedra are connected to four T^2 units through four O^3 positions, while each T^2 tetrahedron is linked to one T^2 (through O^1) and two T^1 tetrahedra (through O^3). The remaining O^2 position is not coshared by another T unit and is therefore a nonbridging oxygen (NBO in the following). As stated, these links lead to the formation of a 2D network in the *ab* plane made up of five-membered rings.

The analysis of the data for the mixed composition Ga2Al1, Ga15Al15, and Ga1Al2 is not trivial since the structure presents two distinct crystallographic sites for Ga and Al, 2*a* (T^1 tetrahedron) and 4*e* (T^2 tetrahedron) with multiplicity ratio 1:2. Therefore, several possibilities are available for the ordering of the two ions on the two sites. The two sites are very similar since they are both tetrahedral with coshared oxygen ions, therefore, a perfect ordering with a strong preference of a given cation for a given site is unlikely. At the same time, the melilite structure is known for the constraints in the connectivity of tetrahedral sites and restrictions in the 2D network linkage, which may lead to specific ordering (e.g., as seen for Co and Si in $Ca_2CoSi_2O_7$ and $Sr_2CoSi_2O_7$).[26] Similar restrictions were also found in the $A_2(Al/Ga)_2SiO_7$ system for which the "Loewenstein rule", predicting that $(AlO_3)-O-(AlO_3)$ linkages are forbidden, is valid.[17,27] The distribution of La and Sr on the M site is assumed to be random, based on the previous analysis.[18]

On the basis of these considerations, all the possible arrangements of the two ions were considered. In principle, three distinct models are possible. For example, for the sample Ga2Al1, the different models taken into account are (1) model A: Ga on site 4*e* with occupancy equal to 1 and Al on site 2*a* with occupancy equal to 1; (2) model B: Ga on sites 4*e* and 2*a*

dx.doi.org/10.1021/jp504829x | J. Phys. Chem. C 2014, 118, 15036−15043

with occupancy 0.5 and Al on site 4*e* with occupancy 0.5; and (3) model C: Ga and Al occupy both sites randomly. Occupancy of Ga for both sites is 0.67, and for Al is 0.33.

The same models were adapted also for the compositions Ga15Al15 and Ga1Al2, by respecting the Ga/Al stoichiometric ratio. Models A and C represent the two extreme cases. Model A is the most ordered one, since it is based on a net preference of Ga and Al for a specific site, whereas C considers a totally random distribution. From the refinements of data using the different structural models, it is possible, in principle, to identify the actual average arrangement of atoms in each sample. In fact, the intensities of the peaks are strongly dependent on the atomic species present in the lattice plane generating the reflection. Since Ga and Al have significantly different neutron cross sections (^{69}Ga 7.88 fm, ^{71}Ga 6.40 fm, and ^{27}Al 3.45 fm), the different models are expected to give different neutron diffraction patterns. Simulations of the neutron diffraction patterns for composition Ga2Al1 based on the three different models are shown in Figure 3 as a representative general case.

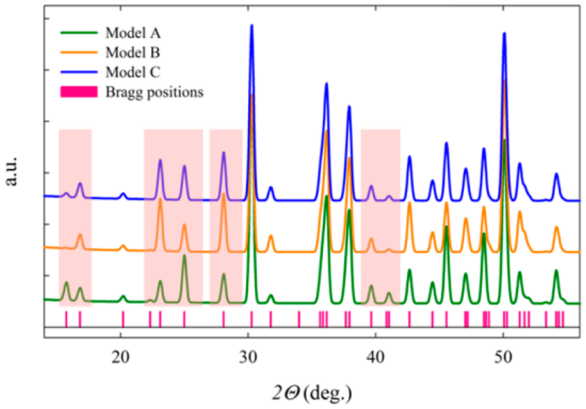

Figure 3. Simulated diffraction patterns based on models A, B, and C for the $LaSrGa_2Al_1O_7$ composition.

The main peak does not show significant intensity changes, whereas the intensities of the peaks at 15.6°, 16.7°, 23.1°, 28.2°, and 41° are predicted to be significantly affected by different arrangements of the Ga/Al cations on the two available sites. Similar results were obtained for the samples Ga15Al15 and Ga1Al2.

The Rietveld refined patterns for Ga2Al1, according to the three models of Figure 3 are presented in Figure 4, together with the results of a fourth refinement (case D) where the occupancies of Ga and Al over the T^1 and T^2 sites are refined starting from model C. The ordered models (A and B) led to significant discrepancies between the calculated and the experimental intensities, whereas the random model C is a better fit to the whole pattern. Very similar results were obtained for the samples Ga15Al15 and Ga1Al2, which implied that for the whole solid solution, no selective preference of Ga and Al for one site was found. Case D differs from model C for the refinement of the occupancies of the 2*a* and 4*e* sites. The refinements led to a small difference in the final occupancies (less than 5%) with respect to the purely random arrangement of model C, with a preference of Ga for site 2*a* and a consequent preference of Al for site 4*e* [final occupancies obtained with case D: Ga(2a) = 0.162 (2), Ga(4e)= 0.338 (2), Al(2a)= 0.088 (2), and Al(4e)= 0.162 (2)]. Also, the distribution of La and Sr over the M site can be considered

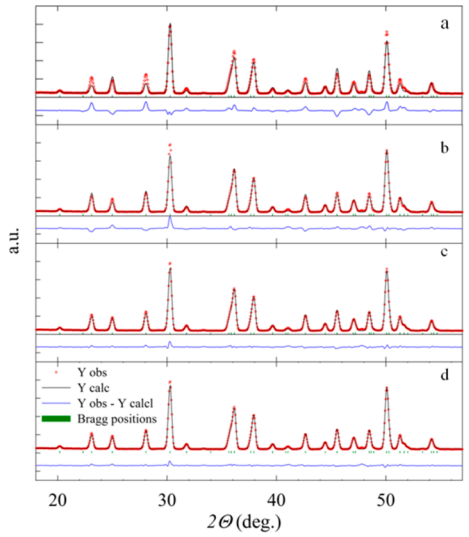

Figure 4. Refinement of powder pattern of $LaSrGa_2Al_1O_7$ according to (a) model A, (b) model B, (c) model C, and (d) model D. Agreement factor for different models: model A: R_{wp} = 10.0, R_p = 7.81, X^2 = 74.5; model B: R_{wp} = 6.68, R_p = 5.32, X^2 = 33.0; model C: R_{wp} = 3.69, R_p = 2.81, X^2 = 11.1; case D: R_{wp} = 3.01, R_p = 2.10, X^2 = 3.21.

as random since no extra peak, indicating the presence of a superstructure, was found in the diffraction patterns. This result is in agreement with our previous findings on the end member $LaSrAl_3O_7$.[18] Both the La/Sr and Ga/Al distributions will be considered as random in the following.

The average structural data (cell parameters, interatomic distances, and anisotropic thermal factors) obtained from the Rietveld refinements were analyzed as a function of the composition. The results are reported in Figure 5. The data for the two end members are in good agreement with the literature.[1,6,18,24] A clear trend of the cell parameters (*a*, *c* and volume) was found with composition. The cell parameters increase when the percentage of Ga ($r_{GaIII(IV)}$ = 0.47 Å) present

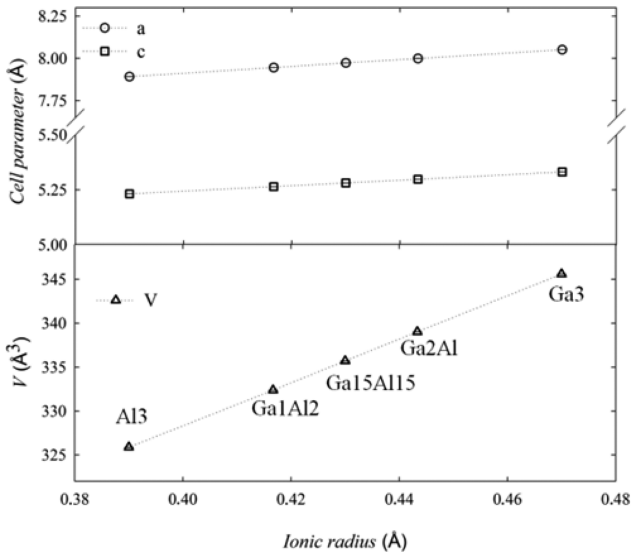

Figure 5. Cell parameters (upper panel) and volume (lower panel) of the whole samples series vs the calculated average ionic radius of the tetrahedral sites obtained from Rietveld refinements. Error bars for experimental values are within the dimension of the symbols.

dx.doi.org/10.1021/jp504829x | J. Phys. Chem. C 2014, 118, 15036−15043

increases with respect to Al ($r_{AlIII(IV)}$ = 0.39 Å).[28] The overall variation is ~2% for *a* and *c* and ~5% for the volume. This effect is due to the dimension of the two ions due to their different ionic radii, since they have the same charge, and changes in oxidation state are not possible. The trend observed for the cell parameters reflects the trend of the interatomic distances T−O, which shows a linear correlation with the composition as reported in Figure 6. All the T−O distances

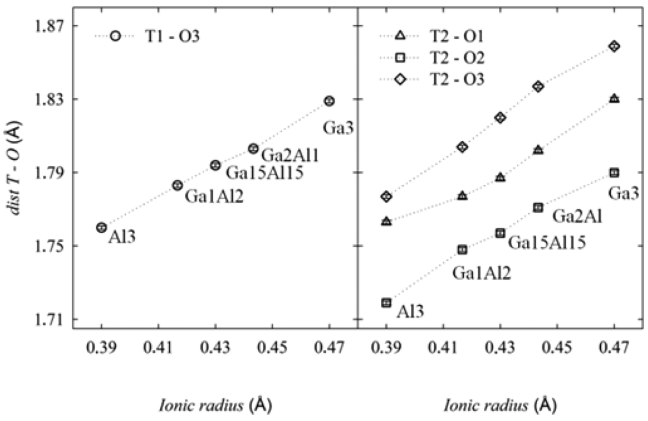

Figure 6. Interatomic T−O distances vs calculated average ionic radius of the tetrahedral sites obtained from Rietveld refinements for the T^1 (left) and T^2 (right) units. Error bars for experimental values are within the dimension of the symbols.

show similar trends with composition, but the overall change in the dimension of T^1 tetrahedra is lower with respect to that of T^2. The difference can be ascribed to the presence of an NBO in the coordination sphere of the T^2 sites.

Our Rietveld analysis helped to shed light on the role played by the two sources of disorder (i.e., La/Sr and Ga/Al mixed sites occupancy) that might generate differences between the average and the local structure. Further information can be obtained by ^{27}Al and ^{71}Ga solid-state NMR. Figure 7, panel a, presents the one-dimensional (1D) ^{27}Al solid-state NMR spectra for the samples with x = 1, 1.5, 2, and 3. The chemical shift range (85−70 ppm) is diagnostic for tetrahedral coordination of the aluminum sites. For the pure Al sample two distinct peaks were observed (see deconvolutions in Figure

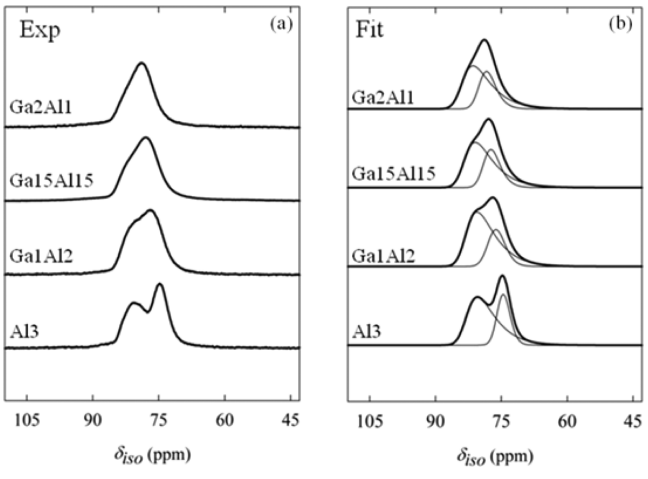

Figure 7. (a) Experimental ^{27}Al spectra for the series of samples and (b) final best-fit results with the single components.

7b and Table 1), which are characterized by different line broadenings. By increasing Ga content, the contribution at high

Table 1. Quadrupolar Parameters from the Fitting Analysis of the 1D ^{27}Al and ^{71}Ga Spectra[a]

sample	site	δ_{iso} (ppm)	C_Q center (MHz)	C_Q width (MHz)	Int. (%)
Al3	Al^2	83.3	6.8	5.0	68.3
	Al^1	75.4	3	3.0	31.7
Ga1Al2	Al^2	83.5	7.0	5.0	74.2
	Al^1	77.6	4.0	3.0	25.8
Ga15Al15	Al^2	83.8	7.0	5.1	67.8
	Al^1	78.7	4.2	3.0	32.4
Ga2Al1	Al^2	84.3	7.0	5.1	66.9
	Al^1	79.7	4.2	4.0	33.1
sample	site	δ_{iso} (ppm)	C_Q center (MHz)	C_Q width (MHz)	Int. (%)
Ga3	Ga^2	232	7.4	4.1	68.3
	Ga^1	223	5.0	3.4	31.7
Ga2Al1	Ga^2	232	8.7	4.0	74.2
	Ga^1	222	5.8	3.5	25.8
Ga15Al15	Ga^2	231	8.9	4.8	67.8
	Ga^1	220	6.5	3.5	32.4
Ga1Al2	Ga^2	229	8.9	4.7	66.9
	Ga^1	218	6.5	3.5	33.1

[a]The agreement factors are above 95% for all the fittings. C_Q width represents the standard deviation of the Gaussian distribution. The quadrupolar asymmetry parameter, η_Q, was kept fixed to 0.5.

field was significantly deshielded, while the chemical shift of the peak at low field was less affected. The overall resolution of the spectra decreased as a result of this different behavior. The assignment of the NMR signals has been already performed for the $LaSrAl_3O_7$ compound, together with an extensive investigation on the correlations between quadrupolar parameters and local structure.[18] The distribution of La and Sr on the available crystallographic site was found to be random; this situation is reflected in the presence of a wide range of possible environments for the Al tetrahedral and thus in a distribution of C_Q values, mainly for the Al2 units in which the surrounding of the nonbridging oxygen, NBO, strongly affect the Al−O distance and thus the symmetry of the Al site. MQMAS spectra were recorded for all the samples of the series and confirm this description of the system as it is possible to distinguish two sites in the range of Al(IV) coordination; the two sites are affected by a distribution in C_Q that leads to a distribution in chemicals shifts reflected in the slope of the two signals (see Figure S1 and caption of the Supporting Inforamation). The peak at around 76 ppm, which is characterized by a quadrupolar coupling constant C_Q in the range of 2−6 MHz, was attributed to the T^1 site, whereas the broader peak (C_Q 2−12 MHz) at around 83 ppm was attributed to the T^2 site. The main difference between the two tetrahedral units is given by the presence of a NBO (O^2) in the coordination sphere of the T^2 site, which is responsible for the increased C_Q.

A substantial linear correlation between the C_Q values and the distance Al^2−O^2 was found, together with a correlation between the Al^2−O^2 distance and the cationic (La/Sr) coordination of the O^2 ions.

In fact, the O^2 ions can be considered tetrahedral coordinated to the T^2 center and to three La/Sr positions, and the ultimate source of the T^2−O^2 bond length variation is

dx.doi.org/10.1021/jp504829x | J. Phys. Chem. C 2014, 118, 15036−15043

the La/Sr local distribution over these last three available positions, as reported in Figure 2b. Low C_Q values corresponded to longer Al^2-O^2 distances, and less distorted tetrahedra, due to more La ions in the O^2 coordination sphere, whereas high C_Q values were related to shorter Al^2-O^2 bonds, and more distorted tetrahedra, due to the greater number of Sr ions in the O^2 coordination sphere.

This picture was considered as the starting point to extract the NMR parameters (C_Q distribution and isotropic chemical shift, δ_{iso}) for the $LaSr(Ga/Al)_3O_7$ series. The best-fit results of the 1D spectra are reported in Figure 7, part b, and in Table 1. The best-fit procedure was based on the use of a Gaussian distribution for C_Q parameters (while η_Q was found to be 0.5 for all the samples), in order to account for the high-field tail generally observed in the ^{27}Al MAS spectra.[29] The substitution of Al with Ga gives a general shift to low field for both the Al^1 and Al^2 peaks. This general trend can be explained by considering the deshielding effect of gallium, which is more electronegative than aluminum. As already stated, the chemical shift of Al^1 peak showed a stronger dependence on the composition than that of Al^2. In principle, this could be rationalized by considering that the T^1 site is connected to four tetrahedra, whereas each T^2 site is connected to only three (see Figure 9), thus the additive contribution to the shift given by the substitution of Al by Ga is higher for the T^1 site, which experiences a larger number of Ga ions in the cationic coordination sphere. However, the observed percentage deviations in the chemical shift (~6% for Al^1 and ~1% for Al^2) cannot be fully explained by simply invoking the additive contributions of the Al-to-Ga substitution, and both the anionic and cationic coordination spheres of the two sites must be considered in detail. Site T^1 is bonded to four O^3 oxygen ions, and no NBOs are present. Around the T^1 polyhedron, four T^2 positions are found together with 8 La/Sr sites. Since the distances T^1-(La/Sr) are larger than the T^1-T^2 distance of ~1 Å, for all the samples Ga2Al1, GA15Al15, and Ga1Al2, the EFG tensor at the Al^1 position is more likely to be influenced by the Ga/Al substitution in the first cationic sphere rather than by the La/Sr arrangement (see Figure 9). This can explain the strong effects on chemical shift along the series, with respect to the pure aluminum sample. The situation is different for the T^2 site, the coordination of which includes the presence of a NBO. The cationic coordination sphere is made up of three T units (one T^2 and two T^1) and 6 La/Sr positions. In this case, the bond distances T^2-(La/Sr) and T^2-T are more similar (with differences less than 0.4 Å), and the EFG tensor is expected to have a stronger dependence on the presence of the NBO and by the La/Sr arrangement (ratio 1:1 for all the samples of the series) than for T^1, in addition to the Ga/Al substitution. This can explain the small changes in chemical shift, which are mainly related to the La/Sr ratio, and only to a less extent to the Ga/Al stoichiometry. Unfortunately, the line widths of both Al^1 and Al^2 peaks are too large to allow separation of the spectral contributions possibly caused by Ga/Al binomial distribution around T^1 and T^2.

Figure 8, panel a, shows the 1D ^{71}Ga spectra of all the samples with $x = 0$, 1, 1.5, and 2 (see also Table 1). Also in this case, all the spectra exhibit a tail at high field, which is more evident in the Ga/Al mixed samples due to the increased local disorder. In this case, however, it was not possible to observe two distinct peaks accounting for the two T sites, due to the severe second-order quadrupole broadening of the central transition, which hides the small crystallographic differences

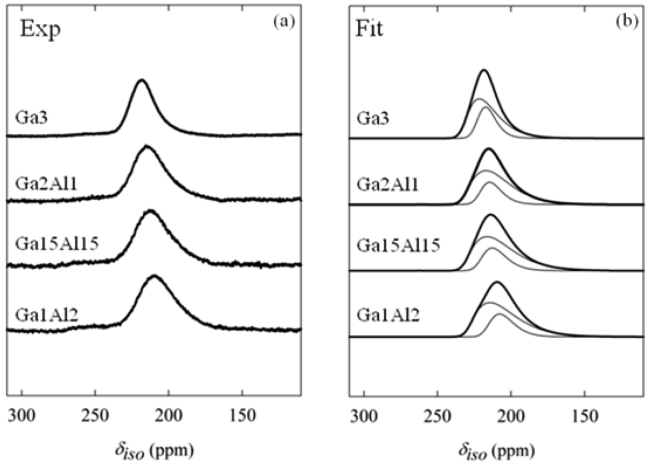

Figure 8. (a) Experimental ^{71}Ga spectra for the series of samples and (b) final best-fit results with the single components.

between the T sites. The use of MQMAS did not give more detailed information (see Figure S2 of the Supporting Information).

Despite the lack of resolution, a best-fit of the spectra was tried on the basis of the results obtained for ^{27}Al (i.e., by postulating the presence of two sites with different C_Q distributions for all Ga spectra). Results are reported in Figure 8, panel b. The chemical shift range (235−220 ppm) confirms the tetrahedral coordination of the gallium ions.[30] Moreover, the ^{71}Ga chemical shifts are in good agreement with those expected on the basis of well-known relationships between ^{71}Ga and ^{27}Al shifts.[31,32] Also in the case of ^{71}Ga NMR, the largest chemical shift variations vs composition are observed for the T^1 site, whereas the shift of the T^2 site is modified at a less extent. These variations can be explained as for the ^{27}Al in terms of the analysis of the composition of the second coordination sphere (Ga/Al or La/Sr). The combined analysis of the chemical shift variations for ^{71}Ga and ^{27}Al can allow the quantification of the effect of Ga/Al substitution. The T^1 is surrounded by four T^2 units (see Figure 9), and so moving from Al3 to Ga3

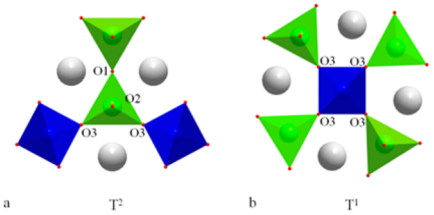

Figure 9. Local environment of the (a) T^2 and (b) T^1 sites. The central tetrahedra are surrounded by the first cationic sphere of La/Sr (gray ions) and Ga/Al sites (T^1 sites in blue, T^2 sites in green).

composition, it is possible to calculate the effect of adding up to four Ga ions on the 4 Al positions in the first cationic coordination sphere. By considering the superposition principle, each Ga ion moves the ^{27}Al chemical shift of the T^1 site of ~1.6 ppm. In case of T^1 tetrahedra, it must be stressed that these average values are obtained by linear interpolation of the chemical shift data reported in Table 1, since the explored samples stoichiometry does not correspond to integer changes in the cationic coordination sphere, except in the case of the Al3 and Ga3 samples. The T^2 site is surrounded only by three T units, in this case the substitutions from 3Al to

dx.doi.org/10.1021/jp504829x | J. Phys. Chem. C 2014, 118, 15036−15043

the final composition 1Al + 2Ga affect the chemical shift of only ~0.40 ppm per cation substitution. Similarly, it is possible to consider the variations of the ^{71}Ga chemical shift. The position of the T^1 site is moved by ~2.3 ppm upon the substitution of each Al with Ga on the four available positions, whereas the T^2 site is shifted by ~1.4 ppm for the variation from 2Al + 1Ga to 3Ga on the first cationic coordination sphere. Also in the case of the T^2 site, where the stoichiometry corresponds to noninteger changes in the cationic coordination sphere, the average shift was obtained by linear interpolation.

CONCLUSIONS

In this work, we reported a new synthetic approach for the $LaSrGa_{3-x}Al_xO_7$ melilite-layered compounds, and addressed the problem to understand the differences between local and average structure by combining neutron diffraction and solid-state NMR. The main results of this study can be summarized as follows. First of all, the average structure could be described by the $P\bar{4}2_1m$ space group that was maintained for the whole series, and the variation of the Ga/Al ratio does not imply changes in the symmetry. Second, two distinct simultaneous sources of disorder were present in the structure: the distribution of La and Sr on M site, and the distribution of Ga and Al on two available T positions. Neutron diffraction data confirm that the distribution of La/Sr and Ga/Al is random, and no evidence of ordering or clustering could be detected. Third, ^{27}Al and, to a lesser extent, ^{71}Ga NMR results allowed us to rationalize the local structure of the T sites in terms of nearest neighbors and next nearest neighbors. The NBO in the T^2 unit was found to be a key element in determining the ^{27}Al NMR spectrum. The detailed analysis of the composition of the first and second coordination sphere for the Al and Ga on the T^1 and T^2 sites leads to a correlation between structure and NMR parameters.

We can state that combination of average and local experimental approaches is a very powerful tool to investigate the subtle differences between local and average order in these complex oxides. The importance of our results is made clearer, considering that such structural details often strongly influence the functional properties of these materials.

ASSOCIATED CONTENT

Supporting Information

Structural data from Rietveld refinements of neutron diffraction patterns and ^{27}Al and ^{71}Ga MQMAS spectra. This material is available free of charge via the Internet at http://pubs.acs.org.

AUTHOR INFORMATION

Corresponding Author

*E-mail: piercarlo.mustarelli@unipv.it.

Present Address

‖Andrew J. Pell, Department of Chemistry, University of Cambridge, Lensfield Road, Cambridge CB2 1EW, U.K.

Notes

The authors declare no competing financial interest.

ACKNOWLEDGMENTS

This project has received funding from the European Union's Seventh Framework Programme for research, technological development, and demonstration under the NMI3-II Grant 283883. We recognize financial support from the Cariplo Foundation through project 2009-2623. A.J.P. and G.P. were supported by the LABEX iMUST (ANR-10-LABX-0064) of the Université de Lyon, within the program "Investissements d'Avenir" (ANR-11-IDEX-0007) operated by the French National Research Agency (ANR).

REFERENCES

(1) Rozumek, M.; Majewki, P.; Schluckwerder, H.; Aldinger, F. Electrical Conduction Behavior of $La_{1+x}Sr_{1-x}Ga_3O_{7-\delta}$ Melilite Type Ceramics. *J. Am. Ceram. Soc.* **2004**, *87*, 1795−1798.

(2) Ryba-Romanowsky, W.; Golab, S.; Pisarski, W. A.; Dominiak-Dzik, G.; Berkowski, M.; Pajaczkowska, A. Investigation of Eu^{3+} Sites in $SrLaGa_3O_7$, $SrLaGaO_4$ and $SrLaAlO_4$ Crystals. *J. Phys. Chem. Solids* **1997**, *58*, 639−645.

(3) Li, M. R.; Kuang, X.; Chong, S. Y.; Xu, Z.; Thomas, C. I.; Niu, H.; Claridge, J. B.; Rosseinsky, M. J. Interstitial Oxide ion Order and Conductivity in $La_{1.64}Ca_{0.63}Ga_3O_{7.32}$ Melilite. *Angew. Chem., Int. Ed.* **2010**, *49*, 2362−2366.

(4) Kuang, X.; Green, M. A.; Niu, H.; Zajdel, P.; Dickinson, C.; Claridge, J. B.; Jantsky, L.; Rosseinsky, M. J. Interstitial Oxide Ion Conductivity in the Layered Tetrahedral Network Melilite Structure. *Nat. Mater.* **2008**, *7*, 498−504.

(5) Tealdi, C.; Mustarelli, P.; Islam, M. S. Layered $LaSrGa_3O_7$-Based Oxide-Ion Conductors: Cooperative Transport Mechanisms and Flexible Structures. *Adv. Funct. Mater.* **2010**, *20*, 3874−3880.

(6) Mancini, A.; Tealdi, C.; Malavasi, L. Interstitial Oxygen in the Ga-Based Melilite Ion Conductor: A Neutron Total Scattering Study. *Int. J. Hydrogen Energy* **2012**, *37*, 8073−8080.

(7) Bao, A.; Tao, C.; Yang, H. Luminescent Properties of Nanoparticles $LaSrAl_3O_7$:RE^{3+} (RE = Eu, Tb) via the Citrate Sol-Gel Method. *J. Mater. Sci: Mater. Electron.* **2008**, *19*, 476−481.

(8) Pracka, I.; Giersz, W.; Swirkowicz, M.; Pajaczkowska, M.; Kaczmarek, S.; Mierczyk, Z.; Kopczynski, K. The Czochralski Growth of $SrLaGa_3O_7$ Single Crystals and Their Optical and Lasing Properties. *Mater. Sci. Eng., B* **1994**, *26*, 201.

(9) Simondi-Teisseire, B.; Viana, B.; Lejus, A. M.; Vivien, D. Optimization by Energy Transfer of the 2.7 μm Emission in the Er:$SrLaGa_3O_7$ Melilite Crystal. *J. Lumin.* **1997**, *971*, 72−74.

(10) Kubota, S. I.; Izumi, M.; Yamane, H.; Shimada, M. Luminescence of Eu^{3+}, Tb^{3+} and Tm^{3+} in $SrLaGa_3O_7$. *J. Alloys Compd.* **1999**, *283*, 95−101.

(11) Zhang, Q.; Wang, J.; Zhang, M.; Su, Q. Tunable Bluish Green to Yellowish Green $Ca_{2(1-x)}Sr_{2x}Al_2SiO_7$:$Eu^{2+}$ Phosphors for Potential LED Application. *Appl. Phys. B: Laser Opt.* **2008**, *92*, 195.

(12) Engelhardt, G.; Michel, D. *High Resolution Solid State NMR of Silicates and Zeolites*; Wiley& Sons: Chichester, 1987.

(13) Kinsley, R. A.; Kirkpatrick, R. J.; Hower, J.; Smith, K. A.; Oldfield, E. High Resolution Aluminum-27 and Silicon-29 Nuclear Magnetic Resonance Spectroscopic Study of Layer Silicates, Including Clay Minerals. *Am. Mineral.* **1985**, *50*, 537.

(14) Gilson, J.-P.; Edwards, G. C.; Peters, A. W.; Rajagopalan, K.; Wormsbecher, R. F.; Roberie, T. G.; Shatlock, M. P. Penta-co-Ordinated Aluminum in Zeolites and Aluminosilicates, *J. Chem. Soc., Chem. Commun.* **1987**, *91*.

(15) Kodama, N.; Takahashi, T.; Yamaga, M.; Tanii, Y.; Qiu, J.; Hirao, K. Long-Lasting Phosphorescence in Ce^{3+}-Doped $Ca_2Al_2SiO_7$ and $CaYAl_3O_7$ crystals. *Appl. Phys. Lett.* **1999**, *75*, 1715.

(16) Kodama, N.; Tanii, Y.; Yamaga, M. Optical Properties of Long-Lasting Phosphorescent Crystals Ce^{3+}-doped $Ca2Al_2SiO_7$ and $CaYAl_3O_7$. *J. Lumin.* **2000**, *87−89*, 1076.

(17) Florian, P.; Veron, E.; Green, T. F. G.; Yates, J. R.; Massiot, D. Elucidation of the Al/Si Ordering in Gahlenite $Ca_2Al_2SiO_7$ by Combined ^{29}Si and ^{27}Al NMR Spectroscopy/Quantum Chemical Calculations. *Chem. Mater.* **2012**, *24*, 4068−4079.

(18) Ferrara, C.; Tealdi, C.; Pedone, A.; Menziani, M. C.; Rossini, A. J.; Pintacuda, G.; Mustarelli, P. Local Versus Average Structure in $LaSrAl_3O_7$: a NMR and DFT Investigation. *J. Phys. Chem. C* **2013**, *117*, 23451−23458.

(19) Hoelzel, M.; Senyshyn, A.; Juenke, N.; Boysen, H.; Schmahl, W.; Fuess, H. High-Resolution Neutron Powder Diffractometer SPODI at Research Reactor FRMII. *Nucl. Instrum. Methods Phys. Res., Sect. A* **2012**, *667*, 32−37.
(20) Rietveld, H. M. Line Profiles of Neutron Powder-Diffraction Peaks for Structure Refinement. *Acta Crystallogr.* **1967**, *22*, 151−152.
(21) Rietveld, H. M. A Profile Refinement Method for Nuclear and Magnetic Structures. *J. Appl. Crystallogr.* **1969**, *2*, 65−71.
(22) Rodriguez-Carvajal, J. FULLPROF: A Program for Rietveld Refinement and Pattern Matching Analysis. *Abstracts of the Satellite Meeting on Powder Diffraction of the XVth Congress of the International Union of Crystallography*, Toulose, France, 1990; IUCr: Chester, England, 1990; p 127.
(23) Kemp, T. F.; Smith, M. E. QuadFit-A New Cross-Platform Computer Program for Simulation of NMR Line Shape from Solids with Distributions of Interaction Parameters. *Solid State Nucl. Magn. Reson.* **2009**, *35*, 243−252.
(24) Thomas, C. I.; Kuang, X.; Deng, Z.; Niu, H.; Claridge, J. B.; Rosseinsky, M. J. Phase Stability Control of Interstitial Oxide Ion Conductivity in the $La_{1-x}Sr_{1+x}Ga_3O_{7-x/2}$ Melilite Family. *Chem. Mater.* **2010**, *22*, 2510−2516.
(25) Skalke, J. M. S.; Herd, R. Crystal Chemistry of $(RE, A)_2M_3O_7$ Compounds (RE=Y, Lanthanide; A=Ba, Sr, Ca; M=Al, Ga). *Powder Diffr.* **1999**, *14*, 195.
(26) Akaki, M.; Tozawa, J.; Akahoshi, D.; Kuwahara, H. Magnetic and Dielectric Properties of $A_2CoSi_2O_7$ (A=Ca, Sr, Ba) Crystals. *J. Phys.: Conf. Ser.* **2009**, *150*, 042001.
(27) Goldsmith, J. R.; Laves, F. Z. Cation Order in Anorthite ($CaAl_2Si_2O_8$) as Revealed by Gallium and Germanium Subsututions. *Z. Kristallogr.* **1955**, *106*, 213.
(28) Shannon, R. D.; Prewitt, C. T. Effective Ionic Radii in Oxides and Fluorides. *Acta Crystallogr.* **1969**, *B25*, 925−946.
(29) Kentgens, A. P. M. A Practical Guide to Solid-State NMR of Half-Integer Quadrupolar Nuclei with Some Applications to Disordered Systems. *Geoderma* **1997**, *80*, 271−306.
(30) Massiot, D.; Vosegaard, T.; Magneron, N.; Trumeau, D.; Montouillout, V.; Berthet, P.; Loiseau, T.; Bujoli, B. ^{71}Ga NMR of Reference Ga_{IV}, Ga_V, and Ga_{VI} Compounds by MAS and QPASS, Extension of Gallium/Aluminum NMR Parameter Correlation. *Solid State Nucl. Magn. Reson.* **1999**, *15*, 159.
(31) Mckenzie, K. J. D.; Smith, M. E. *Multinuclear Solid State NMR of Inorganic Materials*; Pergamon: Amsterdam, 2002.
(32) Bradley, S. M.; Howe, R. F. Correlation Between ^{27}Al and ^{71}Ga NMR Chemical Shifts. *Magn. Reson. Chem.* **1993**, *31*, 883−886.